# Mixed numerical and analytical method for investigating orbital angular momentum beam scattering in turbid water

Austin W. Jantzi
Melanie G. Cockrell
Luke K. Rumbaugh
William D. Jemison

# Mixed numerical and analytical method for investigating orbital angular momentum beam scattering in turbid water

**Austin W. Jantzi,**[a,*] **Melanie G. Cockrell,**[b] **Luke K. Rumbaugh,**[c] **and William D. Jemison**[c]
[a]Clarkson University, Department of Physics, Potsdam, New York, United States
[b]University of Rochester, Institute of Optics, Rochester, New York, United States
[c]Clarkson University, Department of Electrical and Computer Engineering, Potsdam, New York, United States

**Abstract.** A mixed numerical and analytical technique is presented to investigate orbital angular momentum (OAM) beam scattering in turbid water for underwater lidar applications. Electromagnetic simulations are used to generate single-scattering phase functions (SSPFs) that predict the angular scattering distribution for a single particle illuminated by either a Gaussian beam or an OAM beam. These SSPFs are used in array theory and radiative transfer calculations to predict the net volumetric scattering functions (VSFs) and transmittance for multiparticle scattering in a three-dimensional space for both Gaussian and OAM beams. Simulation results show that the VSFs (and therefore the transmittance) of Gaussian and OAM beams are nearly identical, with a slight dependence on OAM charge. Laboratory water tank transmission experiments are performed to verify the simulated predictions. The experimental results are in excellent agreement with the simulation predictions. © *The Authors. Published by SPIE under a Creative Commons Attribution 4.0 Unported License. Distribution or reproduction of this work in whole or in part requires full attribution of the original publication, including its DOI.* [DOI: 10.1117/1.OE.58.4.043104]

Keywords: scattering; orbital angular momentum; underwater lidar; volume scattering function.

Paper 181031SS received Jul. 23, 2018; accepted for publication Apr. 3, 2019; published online Apr. 22, 2019.

## 1 Introduction

Orbital angular momentum (OAM) beams have a nonuniform phase front, which varies linearly from 0 to $2m\pi$, where $m$ is the charge of the OAM beam. This phase front produces an on-axis intensity null in the beam for charge $m > 0$ because of a phase singularity on-axis. Beams with charge $m = 0$ are Gaussian. The use of OAM beams is receiving attention in lidar and communication applications due, in part, to the unique scattering behavior of OAM beams.[1–7] In underwater lidar applications, forward scatter blurs images and backscatter represents unwanted clutter that degrades image contrast and increases receiver shot noise. It has been shown that there is significantly reduced on-axis forward scatter and backscatter from single particles excited by OAM beams when the particle is aligned on/near the OAM beam axis (i.e., when the particle is located at/near the intensity null of the OAM beam).[8] Further investigation is needed to determine if decreased forward scattering and backscattering occur for OAM beam transmission in realistic underwater lidar environments consisting of many randomly located scatterers distributed over long optical path lengths.

To the best of the authors' knowledge, no analytical solution has been derived for OAM beam scattering from single particles and there is little or no published work that predicts OAM beam scattering from multiple particles either analytically or through simulation. Simulated results for a single-scattering phase functions (SSPFs) (i.e., scattering fields) of OAM beams have been reported by Sun et.al.,[8] which show very different scattering behavior for particles on/near the axis of Gaussian beams and OAM beams. Commercially available electromagnetic simulation tools, such as COMSOL, can be used to simulate OAM beam

scattering.[9] While electromagnetic simulation can be used to accurately and efficiently predict scattering from single particles, simulating the scattering behavior from even a moderate number of particles becomes computationally challenging due to the memory and time constraints associated with solving electromagnetically large problems. In this paper, a mixed analytical and numerical method is developed to investigate the volume scattering function (VSF) of OAM beams from multiple randomly located particles. The mixed method uses electromagnetic simulation (COMSOL Multiphysics, RF and wave optics module, electromagnetic waves-frequency domain interface) to compute single-particle SSPF results. This function is then used in an array theory calculation to coherently add the scattering contributions from a large number of particles and generate a net far-field scattering solution, i.e., the VSF. The objective of this approach is to enable accurate prediction of the VSF from OAM beam illumination of many randomly positioned particles, and so predict OAM beam propagation through water turbidities and path lengths that are encountered in underwater lidar. To the best of the authors' knowledge, the results presented here are the first predictions of multiparticle scattering behavior for OAM beams propagating through turbid water over path lengths of practical interest to underwater lidar.

It is important to note that for both Gaussian and OAM beam excitation, a particle's lateral offset from the optical beam axis will determine the SSPF resulting from the excitation. This is because the intensity distribution of the Gaussian beam is spatially nonuniform, and both the intensity and phase distributions of the OAM beam are spatially nonuniform. Especially for OAM beams, this can result in scattering behavior that strongly depends on the particle's position in the beam. For example, when a particle is located on or near the OAM beam axis (i.e., when it is near the OAM

beam intensity null), a reduction in on-axis forward scatter and backscatter is observed. However, as the particle's offset from the OAM null increases, this effect decreases.[8] Single-particle COMSOL simulations are presented in Sec. 2 that illustrate this point and highlight the need to account for this effect in the mixed method.

Section 3 presents an overview of the mixed analytical and numerical method including underlying assumptions and their associated implications on accuracy. Specifically, the mixed method accounts for the previously mentioned spatially dependent scattering excitations by applying an amplitude and phase weighting function to the scattering function to account for each particle's location relative to the beam axis prior to applying array theory.

Section 4 presents VSF calculations generated using the mixed analytical and numerical method for multiple particle scenarios, using both Gaussian and OAM excitations. Two particle scattering scenarios, eight particle scattering scenarios, and a 500 particle scattering scenario are presented. For the two particle and eight particle scenarios, OAM excitation results are validated by comparing the mixed method results with results from full multiple particle COMSOL electromagnetic simulations. For the 500 particle scenario, only the mixed-method results are presented for the OAM excitation since this case is computationally difficult to simulate numerically. The mixed method simulation results show a convergence of the Gaussian and OAM VSFs with increasing turbidity (i.e., particle count) at all angles, including the on-axis forward scatter and backscatter angles that are so different in the case of the single particle near the OAM beam null. This convergence is expected based on an understanding of off-axis single-particle results, as discussed in Sec. 2, the random multiparticle geometry, and the optical wavelength, particle size, and beam waist selected for the simulations.

Section 5 compares simulated transmittance predictions to experimental underwater transmittance measurements obtained by the authors and to results previously published by Cochenour et al.[3] In both cases, the simulated transmittance values are in excellent quantitative agreement with the experimental results. As predicted by the mixed method simulation, the transmittance is nearly identical for the Gaussian and OAM beams for all turbidities, confirming that Gaussian and OAM on-axis forward scatter and backscatter behavior converge for turbidities and path lengths of interest to underwater lidar.

## 2 Numerical Computation of Single-Particle SSPFs

In this section, electromagnetic simulation results are presented for single-particle scattering. Both Gaussian (OAM charge $m = 0$) and OAM charge $m = 1$ cases are presented. While higher order OAM beams could be investigated, the $m = 1$ OAM beam is considered the most practical case of interest for underwater lidar because the $m = 1$ beam will have the least divergence and higher order beams are more difficult to produce experimentally due to the challenge of generating a high-quality rapidly varying phase function.[10] Simulation parameters are chosen to approximate typical underwater lidar conditions. Unless otherwise specified, the following parameters are used in all simulations. The particle size and index of refraction were selected based on the work of Cochenour et al.,[3] who observed that polystyrene beads ($n = 1.598$) with $a = 450$ nm, where $a$ is the particle radius and $n$ is the index of refraction of the material, produce scattering behavior similar to underwater environments ($n_{water} = 1.334$). A linearly polarized laser beam with a beam waist of $w_0 = 10\lambda$ and a wavelength of $\lambda = 532$ nm is used to match typical underwater lidar system laser beam characteristics. A COMSOL electromagnetic simulation is used to solve for the scattered field from a single particle that can be positioned anywhere in the beam. Figure 1 shows the geometry for a single particle in an OAM $m = 1$ beam for two different particle locations. Particle velocity is assumed to be negligible compared to the propagation velocity of the OAM beam. Therefore, static particle locations are used for all simulations in this paper. The average of many instances is used to approximate the scattering of a dynamic volume of particles for the many-particle case.

A background Laguerre–Gaussian electric field is used in all simulations, approximated by
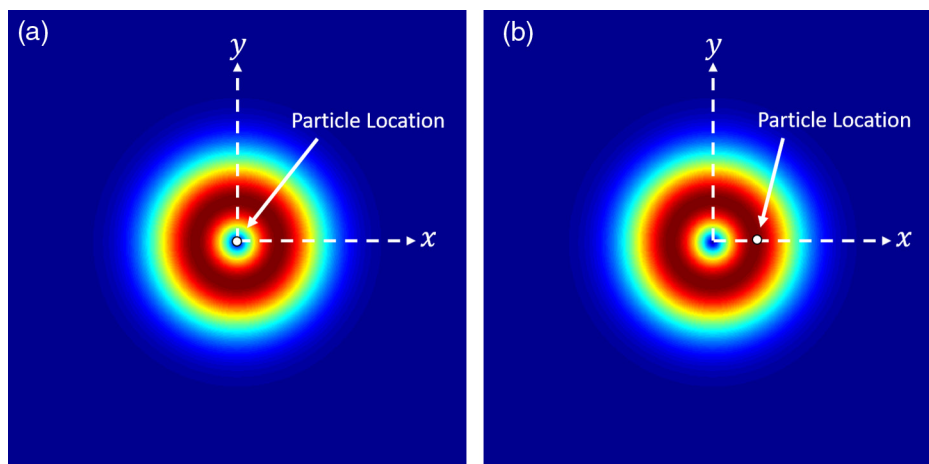


**Fig. 1** Example single-particle OAM excitation scenarios as simulated in Sec. 2. A particle of 900 nm diameter is illuminated by an OAM beam of charge $m = 1$, $\lambda = 532$ nm, and beam waist $w_0 = 10\lambda$. (a) A particle on-axis in the intensity null and (b) a particle off-axis at the beam waist.
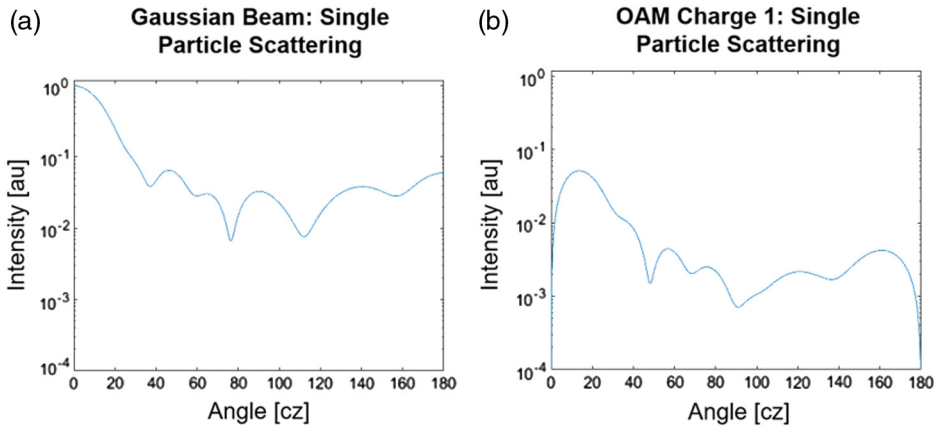
**Fig. 2** COMSOL simulations for both the (a) Gaussian beam and (b) the OAM beam with the particle on the beam axis. For single particles located on the beam axis, the scattering behavior of Gaussian and OAM beams is very different. The ratio of particle radius to wavelength is 0.85.

$$E(r, \phi, z) = \frac{C_{mp}}{w(z)} \left[ \frac{r\sqrt{2}}{w(z)} \right]^{|m|} \exp\left[ -\frac{r^2}{w^2(z)} \right] L_p^{|m|} \left[ \frac{2r^2}{w^2(z)} \right]$$

$$\times \exp\left[ ik\frac{r^2}{2R(z)} \right] \exp(im\phi) \exp[i(2p + |m| + 1)\zeta(z)], \quad (1)$$

where $m$ is the beam charge, $C_{mp}$ is a normalization constant, $L_p^{|m|}$ are the generalized Laguerre polynomials, and $p$ is the radial index. For this study, $p = 0$. This produces a Laguerre–Gaussian beam propagating in the $z$ direction, where $z = 0$ is the location of the beam waist, $w(z) = w_0\sqrt{1 + (z/z_R)^2}$, $z_R = \pi w_0^2/\lambda$, $R(z) = z(1 + (z_R/z)^2)$, and $\zeta(z) = \arctan(z/z_R)$, and $m$ is the OAM charge.

Single-particle scattering behavior for both a Gaussian beam ($m = 0$) and an OAM beam of charge $m = 1$ is shown in Fig. 2 when the particle is located on the beam axis. Consistent with the results of Sun et al.,[8] the OAM-excited SSPF has a null in both the forward and backscattering directions. In general, it is expected that on-axis forward scatter and backscatter will be reduced for single particles located at or near the center null of an OAM beam. This is because the phase singularity that causes the intensity null in the incident beam remains is present in the scattered field. The total scattered intensity is also reduced because the intensity of the OAM beam is lowest at its center and, for the beam and particle geometries of interest in this study, the particle diameter is small compared to the cross-sectional area of the OAM intensity null (as can be seen in Fig. 1).

Both on-axis forward scatter and backscatter increase as the particle is shifted from the beam null to the beam waist. This trend is evident in the numerical results of Fig. 3, which show single-particle SSPFs for an OAM charge $m = 1$ beam as the particle is shifted laterally across the beam waist, from an on-axis location at the beam null to an off-axis location at the beam waist. These results are also consistent with the results of Sun et al.[8]

It is important to note that for our scenarios of interest, the OAM and Gaussian SSPF intensity distributions are almost identical when the particle is located at the maximum intensity point in the respective beam. For the OAM beam, this occurs when the particle is located at the beam waist. For the Gaussian beam, this occurs when the particle is located
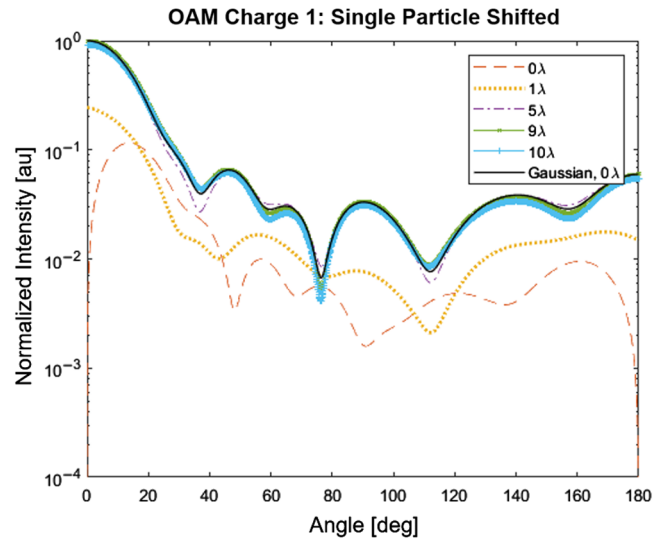


**Fig. 3** COMSOL simulations for an $m = 1$ OAM beam, with the particle shifted 0, 1, 5, 9, and 10 wavelengths from the beam axis. As the particle shifts from the intensity null located at beam axis to the intensity peak located at the beam waist, the scattering pattern resembles the scattering from a Gaussian beam when the particle is located at the intensity which is on the beam axis.

on the beam axis. This observation has implications on the scattering behavior that can be expected from multiple particles, which will be discussed in Sec. 3. Section 3 presents an analytical method for determining the coherent VSF of many particles illuminated by Gaussian and OAM beams.

## 3 Analytical Calculation of Multiparticle VSFs

As demonstrated in Sec. 2, numerical electromagnetic simulation is a reasonable approach for computing the SSPF of complex waveforms incident on single scatterers. However, electromagnetic simulation is not an efficient approach for calculating the multiparticle VSF for many particles because of the computational demands of this electrically large problem. In this section, an analytical method is presented to accurately compute the coherent VSF from a three-dimensional (3-D) array of particles. Section 4 presents VSFs for multiparticle scenarios using the SSPFs computed

numerically in Sec. 2 and the analytical method presented here.

Array theory states that for a 3-D array of identical apertures, the far-field is as follows:

$$E(X, Y, Z) = \sum_{i=1}^{N} \iiint_{-\infty} A_i(x', y', z')$$

$$* e^{ik[X(x_i + x') + Y(y_i + y') + Z(z_i + z')]/R} dx' dy' dz', \quad (2)$$

where $N$ is the number of particles, $X$, $Y$, and $Z$ are the far-field co-ordinates, $x$, $y$, and $z$ are the near-field co-ordinates. The far-field is projected onto a spherical surface that has a radius of $r = R$ from the origin,[11] as shown in Fig. 4. In this study, $\theta = 0$ and the beam propagates along the $z$ axis. $A_i(x', y', z')$ is the 3-D near-field aperture function, which is the electric near-field associated with the SSPF in Sec. 2.

To calculate the far-field scattering intensity (i.e., the VSF) for multiple particles, following Hecht,[11] Eq. (2) becomes

$$I(k_x, k_y, k_z) = \sum_{i=1}^{N} \left[ \mathcal{F}\{A_i\}^2 + \sum_{j=i+1}^{N} \mathcal{F}\{A_i\} * \mathcal{F}\{A_j\} \right.$$

$$\left. \times \cos(k_X \Delta x + k_Y \Delta y + k_Z \Delta z + \Delta \delta) \right], \quad (3)$$

where $\mathcal{F}\{A\}$ is the Fourier transform of $A_i$, $k_0 = \frac{2\pi}{\lambda}$, $k_X = k_0 \sin \theta \sin \phi$, $k_Y = k_0 \sin \theta \sin \phi$, $k_Z = k_0 \cos \phi$, $\Delta x = x_i - x_j$, $\Delta y = y_i - y_j$, $\Delta z = z_i - z_j$, and $\Delta \delta = \delta_i - \delta_j$. $\mathcal{F}\{A\}$ is the electric far-field SSPF, and $\mathcal{F}\{A\}^2$ is the SSPF. For Gaussian beams and plane waves, $\Delta \delta = \Delta z \frac{\lambda}{n}$, which accounts for the phase difference due to propagation in $z$. For OAM beams, this term must be modified to account for both the phase difference due to propagation in $z$ and the phase difference due to the particle's position on the nonuniform OAM phase front. For OAM beams, $\Delta \delta = \Delta z \frac{\lambda}{n} + (m \arctan \frac{y_i}{x_i} - m \arctan \frac{y_j}{x_j})$. This phase shift must be considered when evaluating propagation differences between
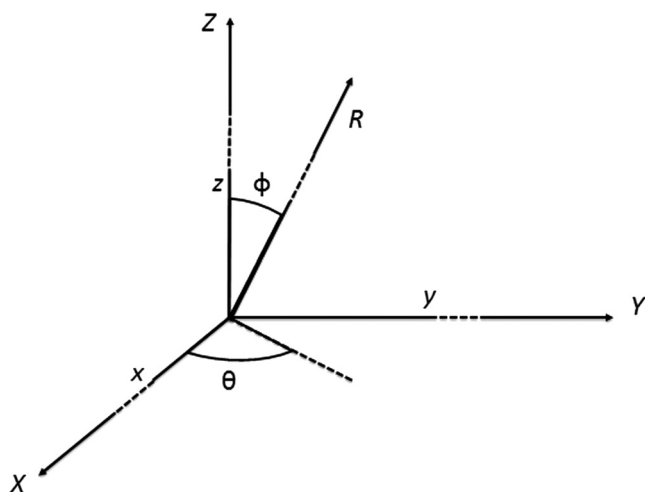


**Fig. 4** The geometry used for the analytical method.

Gaussian and OAM beams due to the nonuniform phase front of OAM beams with order $m > 0$.

In general, $A_i$ is calculated for each particle using the full electromagnetic simulation. However, two assumptions are made in the analytical method that simplify the specification of $A_i$.

**Assumption 1:** The propagating beam is not significantly distorted by the scatterers. That is, each scatterer is interacting with a beam that has not been perturbed.

**Assumption 2:** For particles that are small relative to the beam waist, the incident field on each particle is nearly a plane wave. The intensity and phase of the incident plane wave will be computed as the average intensity and phase of the actual incident beam (i.e., Gaussian or OAM) at the particle's location in the beam front. No phase or intensity gradients will be considered across a given particle.

Given these assumptions, $A_i$ can be determined from a plane wave scattering function that can be computed analytically via Mie theory[12] or from a single-particle plane wave scattering electromagnetic simulation. Assumption 1 becomes less valid as the propagation length in $z$ increases, and Assumption 2 becomes less valid as the ratio of $w_0$ to the particle radius decreases. It is noted that $A_i$ can be determined from single-particle electromagnetic simulation results, which helps maintain accuracy under conditions when the two previously stated assumptions become less valid. Small volumes are simulated to generate the VSFs, so that Assumption 1 is reasonable. Also, for the simulations in the following section, $a = 450$ nm and $w_0 = 10$ $\lambda = 5320$ nm, yielding a sufficiently high ratio of beam waist to particle radius so that Assumption 2 is reasonable. The $A_i$ SSPFs are determined from single-particle plane wave scattering simulation. Since we are using a numerically computed $A_i$ within the analytical array theory calculation to generate the VSF, we refer to our approach as a mixed numerical and analytical method, or simply a "mixed" method.

At this point, it is constructive to predict whether or not the VSF distribution of Gaussian and OAM beams will be similar based on an understanding of the single-particle scattering results of Sec. 2 and the VSF equation presented in this section. It is reasonable to assume that in a multiple-particle scenario, the majority of the total scattering energy will be associated with scattering from particles that are located at or near the Gaussian or OAM beam intensity peak. Section 2 demonstrated that the SSPF intensity distributions are nearly identical for OAM and Gaussian beams when the particles are located at their respective beam peaks. Therefore, for either the Gaussian or OAM case, the total scattered field will be the coherent addition of individual scattering events that have SSPFs that are largely independent of beam type. Any coherent interference from these individual identically distributed scattering events will occur due to the cosine term in the second summation of Eq. (3). The argument of this cosine term includes phase terms $k_X \Delta x$, $k_Y \Delta y$, and $k_Z \Delta z$, which are based on the physical locations of the particles and, therefore, are independent of beam type, as well as the beam phase front term, $\Delta \delta = \Delta z \frac{\lambda}{n} + (m \arctan \frac{y_i}{x_i} - m \arctan \frac{y_j}{x_j})$, which is highly dependent on beam type. The random locations of the particles will result

in positional phase terms that can be described by random variable that is uniformly distributed between 0 and modulo $2\pi$. Likewise, the beam front terms for the Gaussian and OAM beams are derived based on the random particle locations. Therefore, they also will be random variables that are uniformly distributed between 0 and modulo $2\pi$. It follows that the argument of the cosine term is a random variable that is uniformly distributed between 0 and modulo $2\pi$, which results in the expectation of the VSF interference term being zero. As a result, neither the positional location of the particles nor the phase distribution of the incident beam front significantly changes the VSF for a random volume of particles. Of course, significant interference effects can occur due to the particle position and the beam phase front for a small number of purposely spaced scatters. The next section presents the results of the mixed method for particles illuminated by Gaussian and OAM beams that demonstrate this behavior.

## 4 VSF Simulations using the Mixed Analytical and Numerical Method

In this section, VSF simulation results obtained using the mixed method are presented for several multiple particle scenarios for both Gaussian ($m = 0$) and OAM charge ($m = 1$) excitations. These simulations use the SSPFs computed numerically in Sec. 2 with the analytical calculations from Sec. 3 to generate the VSF. Prior to describing these results, it is noted that results from multiparticle mixed method simulations were first compared to multiparticle results reported in the literature that used both plane wave and Gaussian excitations.[13–15] While mixed method plane wave and Gaussian results will not be presented here, they were in excellent agreement with the results reported in the literature.

### 4.1 VSF for Two Particles

The two particle case (or, $N = 2$, where $N$ is the number of particles) is the simplest multiparticle case to consider. It is also a problem that can be solved readily through electromagnetic simulation. Both the mixed method and COMSOL were used to simulate scattering from two particles located in the $xy$ plane. The particles are separated by $\Delta x = 6\lambda$, $\Delta y = 0$. In this case, Eq. (3) becomes:

$$I(k_x, k_y, k_z) = \mathcal{F}\{A_1\}^2 + \mathcal{F}\{A_2\}^2 + \mathcal{F}\{A_1\}$$
$$* \mathcal{F}\{A_2\} \cos(6\lambda k_0 + \pi), \qquad (4)$$

where $\Delta\delta = \pi$ because of the nonuniform phase front of the $m = 1$ OAM beam. For a Gaussian beam, $\Delta\delta = 0$ produces a result similar to double slit interference. However, the intensity envelope is now the scattering function of a single particle rather than a sinc function as is the case for double slit interference. The results for both the Gaussian beam and the OAM beam are shown in Fig. 5. This simple case maintains the null generated in the on-axis forward scatter direction and increases side scatter as observed by Sun et al.[8] Just as the Gaussian case produces results like the double-slit experiment, the results for the OAM beam are similar to an OAM beam incident on a double slit.[16] Further, there is an excellent agreement between the mixed method and the COMSOL simulation results.

### 4.2 VSF for Several Particles

Next, scattering from $N = 8$ particles is considered. Two scenarios were considered: one where all particles were located in the same plane and the other where the particles were randomly distributed in a volume. In all cases of a random distribution, the distribution is uniform. Both of these $N = 8$ cases can be solved numerically, allowing a full electromagnetic simulation to again serve as a benchmark against which to validate the mixed method results.

In the first $N = 8$ case, the particles are randomly distributed in a $50\lambda \times 50\lambda$ region of the $xy$ plane, and the results generated in COMSOL are plotted with results generated by the mixed method in Fig. 6. In the second case, the particles are randomly distributed in a $50\lambda \times 50\lambda \times 50\lambda$ cube, and the results from COMSOL simulation and the mixed method are plotted in Fig. 7. In the case of particles in the $xy$ plane, there remains reduced intensity of the on-axis forward scatter. However, as $\Delta z$ increases and the simulation better represents the underwater environment, the forward scatter null is less pronounced. In both cases, the agreement between the mixed results and COMSOL results is excellent. For the case of a plane of particles in the $xy$ plane, the root mean squared error (RMSE) for the mixed method compared to COMSOL simulated results is 0.17%. The RMSE for the
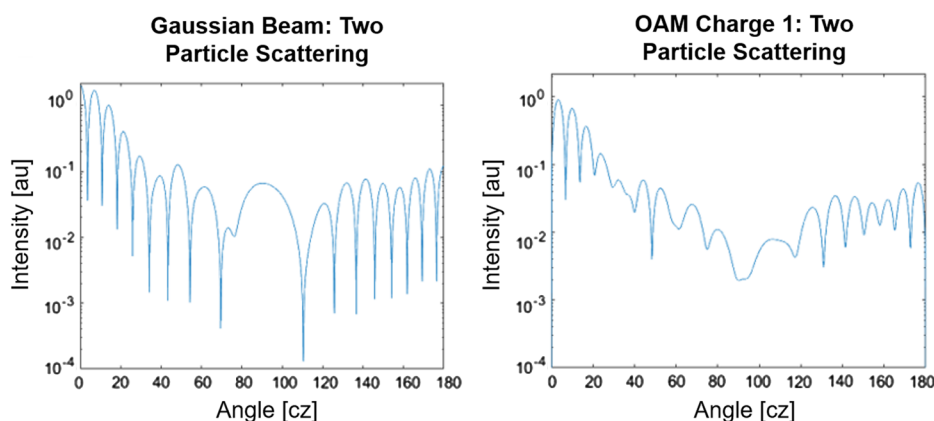


**Fig. 5** COMSOL simulations of two-particle scattering for both (a) the Gaussian beam and (b) the OAM beam. Reduced intensity at scattering angles of 0 deg, and 180 deg is still present for the OAM case.
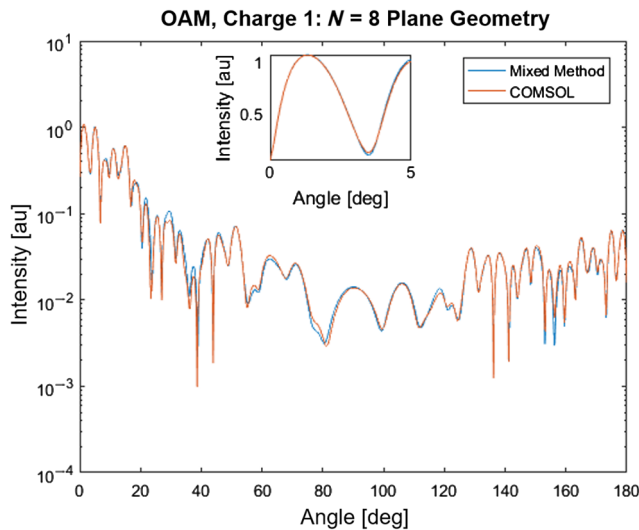
**Fig. 6** Results of the mixed method and COMSOL simulation for $N = 8$ particles randomly distributed in the $xy$ plane. There is a good agreement between the COMSOL simulation and the mixed method.
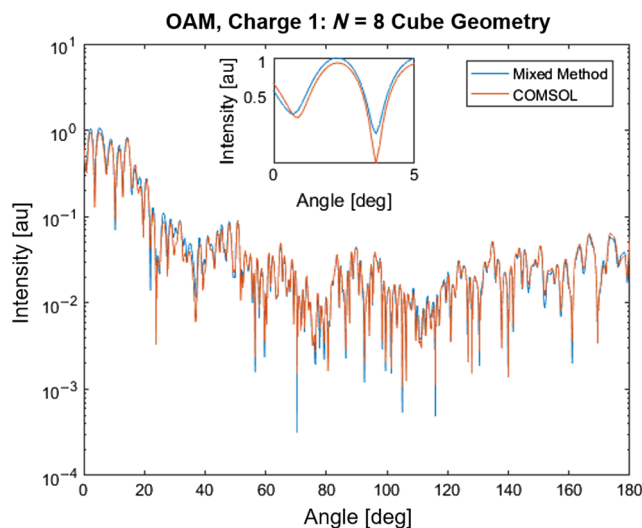


**Fig. 7** Results of the mixed method and COMSOL simulation for $N = 8$ particles randomly distributed in a cube. There is a good agreement between the COMSOL simulation and the mixed method.

volume of particles is 0.46%. While still very low, the higher error in the volumetric scenario is consistent with Assumption 1 (i.e., the beams exciting the particles in the volume will be perturbed as $z$ increases). The mixed method significantly reduces the computational cost. The run time for the COMSOL simulations on 32-core, 128 GB workstation was 540 s, while the mixed method had a run time of 0.02 s.

### 4.3 *VSF for Many Particles*

In this section, mixed method simulation results of the VSF for $N = 500$ particles are shown. A full COMSOL simulation is now impractical because of computational time and memory constraints, so only the mixed method results are
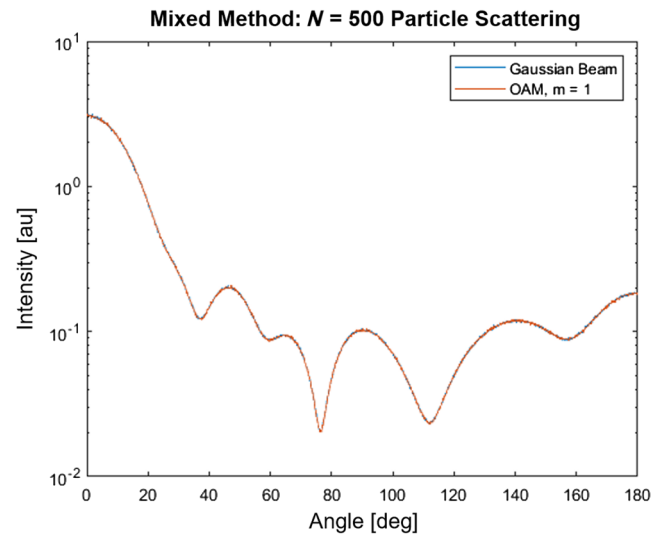


**Fig. 8** Results of the mixed method for both the plane wave and the OAM beam. For many particles, the forward scatter null is not observed and there is little difference between the scattering behavior of OAM beams and Gaussian beams. Note: This geometry is not practical for a COMSOL simulation.

presented. The position of the particles is randomly generated in a $50\lambda \times 50\lambda \times 1000\lambda$ volume. Each result represents the average of 2000 simulations, where the random particle locations are reseeded for each simulation. VSF results for a Gaussian beam and an OAM charge $m = 1$ beam are shown in Fig. 8. The null in on-axis forward scatter and backscatter that is seen in the single and few particle VSFs for the OAM beam has disappeared, and the OAM VSF is now almost identical to the Gaussian VSF. This is consistent with the observations made in Sec. 2, where it was noted that the majority of the OAM scattering energy would be from particles whose SSPF intensities were similar to a Gaussian SSPF intensity.

To verify that the VSF of Gaussian and OAM beams converge, different particle sizes and charges were used in the mixed numerical and analytical method. Specifically, particle sizes, $a = 35.8$ nm, $a = 450$ nm, and $a = 707$ nm, were investigated. In all of these cases, the particle is small compared to the beam waist. The VSF results are shown in Fig. 9, and the forward and backscattering nulls are no longer present. OAM beam charges $m = 1$, $m = 2$, and $m = 16$ were also simulated for $N = 500$ particles. Each VSF is nearly identical to the Gaussian VSF, and the results are shown in Fig. 10.

These results are expected from what was previously shown. In Sec. 2, it was shown that the angular scattering pattern is likely to be the same for Gaussian and OAM beams. In Sec. 3, it was shown that the phase distribution of the OAM beam will not significantly impact the average VSF. Now, it is apparent that the total scattering energy will also be nearly the same for different OAM charges. This is because as the OAM charge increases, the radius and area of the high-intensity "ring" portion of the OAM beam's spatial profile increase. The average intensity in that ring necessarily decreases. Thus, high-charge OAM beams may interact with more particles but with a lower average intensity per interaction.

**Mixed Method: *N* = 500 OAM Charge 1 Scattering**
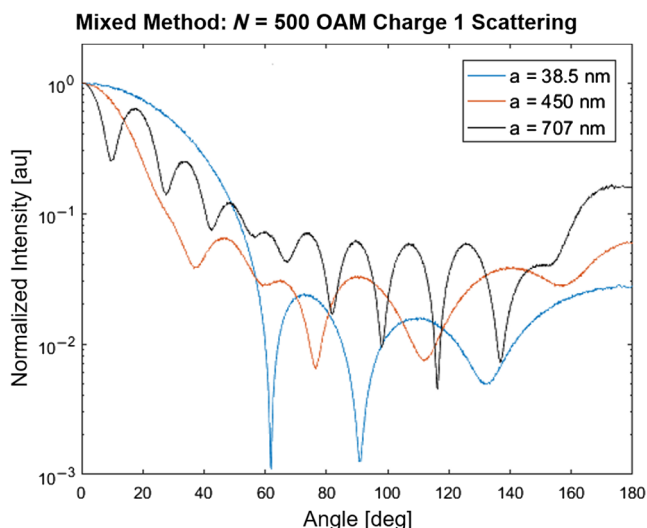


**Fig. 9** Results of the mixed method for OAM beams with particle sizes $a = 35.8$ nm, $a = 450$ nm, and $a = 707$ nm. Results are normalized to focus on changes in forward scattering behavior. The scattering behavior for OAM beams is as expected from a Gaussian beam.

**Mixed Method: *N* = 500 Particle Scattering**
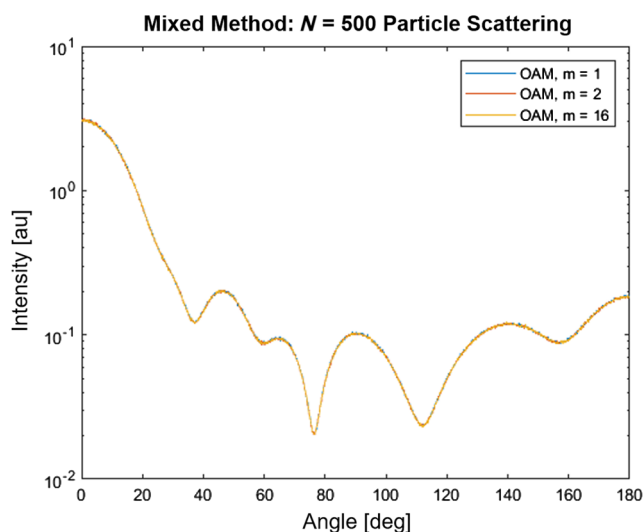


**Fig. 10** Results of the mixed method for OAM beams of charge $m = 1, 2, 16$. For many particle scenarios, increasing the charge does not significantly change the total intensity of the VSF.

## 5 Comparison to Propagation Experiments

In this section, experimental underwater optical transmission experiments from both Gaussian and OAM charge $m = 1$ beams are presented and compared to predictions from the mixed method simulations. Simulation results are also compared to experimental results from Cochenour et al.[3] The transmission experiments reflect the effects of forward scattering as a function of turbidity.

### 5.1 Experimental Setup

The underwater transmission measurement experimental setup is shown in Fig. 11. A 25-mW Nd:YAG 532 nm laser is used as the light source. Lenses L1 and L2 are used to expand the beam to fill the active area of the spatial-light modulator (SLM) (HoloEye Pluto2 VIS-020), which is used to produce the phase profiles necessary to generate different OAM charges. A polarizer is used to horizontally polarize the beam and align it with the polarization axis of the SLM. The beam was transmitted through a $z = 7.32$ m water tank. The beam waist is $\sim 5000$ $\mu$m. Equate maximum strength antacid is used to increase the turbidity of the water, as is common in underwater studies.[3] The absorption and total attenuation coefficients are monitored simultaneously with a WET Labs ac-s *in-situ* spectrometer and a Sequoia Scientific LISST-200X measured the particle sizes. A Hamamatsu H10435 photomultiplier tube (PMT) with an active area of 25 mm is used as the receiver. The receiver field-of-view is $\sim 5$- deg half angle, and the measurement time is 1 s.

### 5.2 Simulated Transmission Setup

In order to simulate transmission results to compare to the measured results, the radiative transfer equation (RTE) with small angle approximations is used. The RTE depends only on the VSF and properties of the scatterers and the system [e.g., field-of-view (FoV)]. As shown in Sec. 4, the VSF is nearly identical for charges $m = 0$ and $m = 1$. Thus, it is expected that the transmittance will be nearly identical for both beams. The transmitted intensity is calculated using:

$$I_T = I_u + I_s, \tag{5}$$

where $I_T$ is the transferred intensity, $I_u$ is the unscattered intensity, and $I_s$ is a correction term for the collected scattered intensity.[17] $I_u = \exp(-cz)$ is given by Beer–Lambert's law. With the small angle approximation:
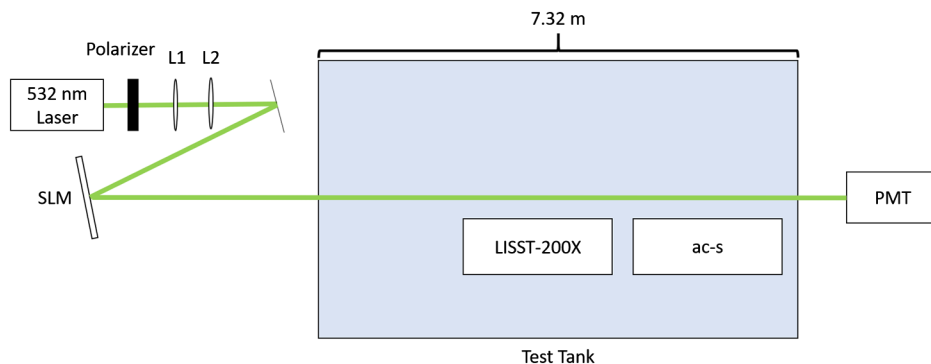


**Fig. 11** Experimental setup: the SLM is used to transmit beams with different OAM charges, Equate antacid is used to increase the turbidity, and the PMT measures the power of the transmitted beams.

$$I_s = 2I_0 \pi b z \, \exp(-\alpha z) \int_0^\psi p(\theta) \sin(\theta) \mathrm{d}\theta, \qquad (6)$$

where $p(\theta)$ is the VSF, $I_0$ is the initial intensity and is normalized to unity, $b$ is the scattering coefficient and $\alpha$ is the absorption coefficient. These coefficients are determined from the 0.85 scattering albedo of antacid[18] and they scale with particle concentration. The integral accounts for the scattered light collected by the detector, where $\psi$ is the half angle of the detector FoV, and $\exp(-az)$ accounts for the absorption of the scattered light. The VSF is generated using the mixed method for particles of $a = 1450$ nm (the mean experimental particle size, as measured using the LISST) for a fixed volume of particles and increasing particle densities corresponding to attenuation lengths between $cz = 0.1$ and $cz = 30$. The particle count for the volume is determined using the relation between the attenuation coefficient, $c$, and the number of particles, $N$: $c = \sigma \frac{N}{V}$, where $\sigma$ is the attenuation cross-section of the particle.

### 5.3 Experimental and Simulated Results

Transmission measurements are made at each turbidity for transmitted beams of charge $m = 0$ and $m = 1$. The transmittance is calculated as the ratio of the input power and the output power and is plotted with increasing turbidity in Fig. 12. The simulated transmittance using phase functions generated using the mixed method and the RTE is also plotted. As turbidity increases, there is almost no difference in the transmittance of the different charges and they are in excellent agreement with the simulated results. This suggests that there is no significant difference in Gaussian and OAM charge $m = 1$ on-axis forward scattering for the case of many randomly located particles, as predicted by the mixed method in Sec. 4.

Next, the transmittance is simulated for the experimental parameters (i.e., particle size, albedo, and FoV) described by
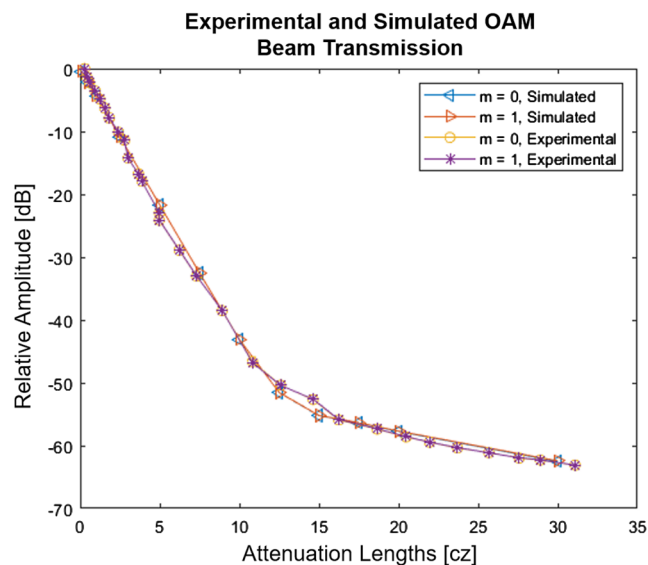


**Fig. 13** Simulated results for antacid and polystyrene beads with experimental parameters are in good agreement with Cochenour et al., with OAM charges, $m = 0,1,16$. A slight increase in transmittance is observed with increasing charge. The inset shows details for beads at high turbidity.

Cochenour et al.[3] for charges $m = 0$, $m = 1$, and $m = 16$. The simulated transmittance using phase functions generated using the mixed method and the RTE is plotted in Fig. 13. Overall, the simulated results are in good agreement with the experimental results of Cochenour et al. A slight increase in the simulated transmittance at higher turbidities is observed for increasing OAM charge. This difference in transmittance with OAM beam order is believed to be related to the structure of the incident beam intensity profiles, $|E(r, \theta, z)|$, which are OAM charge dependent. This effect was also observed by Cochenour et al.; however, the difference reported by Cochenour et al. was on the order of 2 to 3 dB compared to the <1 dB difference observed in our simulation and seen in the inset of Fig. 13. A possible reason for the discrepancy between the simulated results and the experimental results in the transmittance as a function of beam order is some difference between the theoretical intensity distributions of the simulated OAM beams and the actual intensity distributions of the experimentally produced OAM beams. Further investigation is needed to be certain of the cause(s) of this effect.

## 6 Conclusion

OAM beams have been receiving much attention in the lidar community due to their unique scattering characteristics. Much is known about OAM scattering from single particles; however, less is currently known or understood about OAM propagation and scattering in turbid underwater environments, which are very different from the single scattering case.

A mixed numerical and analytical technique was presented that accurately predicts volumetric scattering from Gaussian and OAM beams for realistic underwater lidar scenarios. Mixed method results were compared to previously published results and, in a few limited cases, to full electromagnetic simulations. The mixed method significantly reduces the computational cost of calculating scattering



**Fig. 12** The fraction of light transmitted through the test tank as turbidity increases for various OAM charges, $m = 0$ and $m = 1$, where a charge of zero is a Gaussian beam plotted with simulated predictions of transmission. There is almost no difference in the transmission of the different beams and excellent agreement with simulation.

behavior compared to a full electromagnetic simulation approach. This enables high turbidity scenarios to be investigated that otherwise would be impractical to explore. Mixed method results were also compared to results from an underwater transmission experiment performed by the authors and previously reported experimental results from the literature. In all comparison cases, excellent agreement was achieved. To the best of the authors' knowledge, this is the first reported prediction of OAM beam propagation in turbid water at turbidities and path lengths of interest to underwater lidar.

For the underwater lidar scenarios presented, there is not a substantial difference in propagation behavior between OAM and Gaussian beams. In Sec. 2, it was shown that the angular scattering distribution for OAM and Gaussian beams is very similar. In Sec. 3, it was shown that the spatial phase of OAM beams does not significantly impact the VSF. In Sec. 4, it was shown that the scattering energy is nearly identical for each studied charge. In Sec. 5, it was shown that this leads to little difference in propagation behavior.

It should be noted that there are potential advantages to using the spatial characteristics of OAM beams for communications and coherence discrimination, which can potentially increase system performance.[1,2,5–7] Further, no claims are made about the propagation behavior of OAM beams in other applications (such as terrestrial lidar and remote sensing) since these scenarios were not the subject of this study, and virtually all of the relevant parameters (wavelength, beam diameter, particle size, density, etc.) will be different.

## Acknowledgments

## References

1. J. Baghdady et al., "Multi-gigabit/s underwater optical communication link using orbital angular momentum multiplexing," *Opt. Express* **24**, 9794–9805 (2016).
2. J. Baghdady et al., "Blue-light digital communication in underwater environments utilizing orbital angular momentum," *Proc. SPIE* **9827**, 98270G (2016).
3. B. Cochenour et al., "Propagation of modulated optical beams carrying orbital angular momentum in turbid water," *Appl. Opt.* **55**, C34–C38 (2016).
4. W. B. Wang et al., "Deep transmission of Laguerre–Gaussian vortex beams through turbid scattering media," *Opt. Lett.* **41**(9), 2069–2072 (2016).
5. W. Sun et al., "Technique to separate lidar signal and sunlight," *Opt. Express* **24**(12), 12949–12954 (2016).
6. J. Baumgartl et al., "Optical path clearing and enhanced transmission through colloidal suspensions," *Opt. Express* **18**(16), 17130–17140 (2010).
7. A. Jantzi et al., "Enhanced underwater ranging using an optical vortex," *Opt. Express* **26**(3), 2668–2674 (2018).
8. W. Sun et al., "A FDTD solution of scattering of laser beam with orbital angular momentum by dielectric particles: far-field characteristics," *J. Quant. Spectrosc. Radiat. Transfer* **188**, 200–213 (2017)
9. COMSOL, *COMSOL Multiphysics RF Module User's Guide Manual, Version 5.0*, COMSOL, Inc., Stockholm, Sweden (2018).
10. E. Rueda et al., "High-quality optical vortex-beam generation by using a multilevel vortex producing lens," *Opt. Lett.* **38**(19), 3941–3944 (2013).
11. J. Hecht, *Optics*, Laser Light Press, Auburndale, Massachusetts, pp. 519–556, (2015).
12. G. Mie, "Beigrade zur optik truber medien, speziell kolloidaler metal-losungen," *Ann. Phys.* **330**, 377–445 (1908).
13. A. K. Hamid, I. R. Ciric, and M. Hamid, "Radar cross section of an array of dielectric spheres," in *Symp. Antenna Technol. Appl. Electromagnet.* (1990).
14. Y. Han and Z. Wu, "Scattering of a spheroidal particle illuminated by a Gaussian beam," *Appl. Opt.* **40**(15), 2501–2509 (2001).
15. D. W. Mackowski and M. I. Mishchenko, "Direct simulation of multiple scattering by discrete random media illuminated by Gaussian beams," *Phys. Rev. A* **83**(1), 013804 (2011).
16. R. Liu et al., "Characterizing the phase profile of a vortex beam with angular-double-slit interference," *J. Opt.* **15**(12), 125712 (2013).
17. L. Wind and W. W. Szymannski, "Quantification of scattering corrections to the Beer-Lambert law for transmittance measurements in turbid media," *Meas. Sci. Technol.* **13**, 270–275 (2002).
18. L. Mullen et al., "Amplitude-modulated laser imager," *Appl. Opt.* **43**(19), 3874–3892 (2004).

**Austin W. Jantzi** is a graduate student at Clarkson University. He received his BS degree in physics from Grove City College in 2016. His current research interests include orbital angular momentum, optical coherence detection, and optical wavefront processing. He is a member of SPIE.

**Melanie G. Cockrell** is a graduate student at the University of Rochester's Institute of Optics. She received her BS degree in electrical engineering and physics from Clarkson University in 2018. Her undergraduate thesis work investigated the far-field scattering behavior of Laguerre–Gaussian beams for underwater applications using numerical simulation methods.

**Luke K. Rumbaugh** is the director of the Underwater Lidar Lab at Clarkson University. He received his BS degree from Grove City College, and his MS and PhD degrees in electrical engineering from Clarkson University. His current research interests include 3-D vision, underwater optics, and high-resolution lidar systems. He is a member of SPIE, IEEE, and the Marine Technology Society.

**William D. Jemison** is the dean of the Coulter School of Engineering at Clarkson University. He received his BS degree from Lafayette College, MS degree from Penn State University, and his PhD degree in electrical engineering from Drexel University. His current research interests include microwave photonic systems, lidar systems, and wireless and optical communications systems. He is a fellow of the IEEE.